Spatially coordinated collective phosphorylation filters spatiotemporal noises for precise circadian timekeeping

Seok Joo Chae[1,2], Dae Wook Kim[3], Seunggyu Lee[2,4], Jae Kyoung Kim[1,2,5,*]

[1] Department of Mathematical Sciences, Korea Advanced Institute of Science and Technology, Daejeon, 34141, Republic of Korea

[2] Biomedical Mathematics Group, Institute for Basic Science, Daejeon, 34126, Republic of Korea

[3] Department of Mathematics, University of Michigan, Ann Arbor, MI, 48109, USA

[4] Division of Applied Mathematical Science, Korea University, Sejong, 30019, Republic of Korea

[5] Lead Contact

*Correspondence: jaekkim@kaist.ac.kr

Graphical Abstract

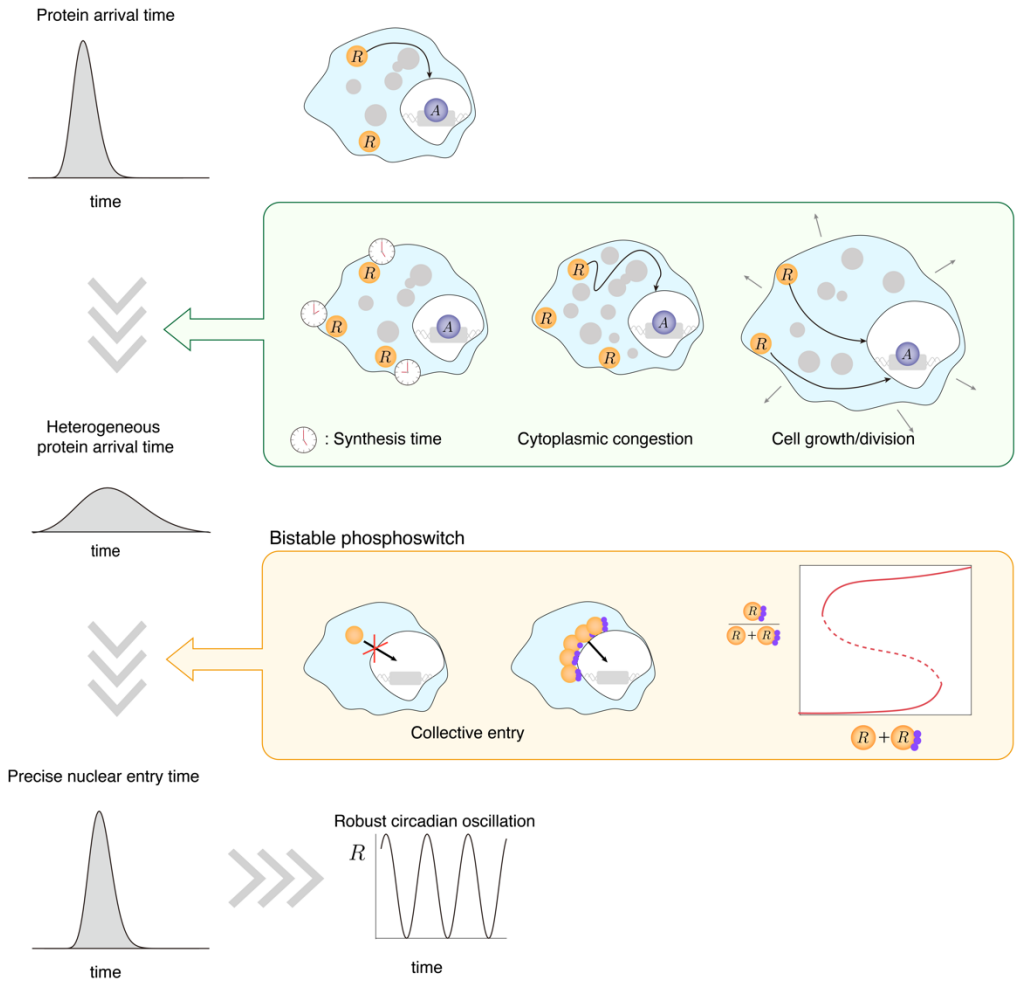

Highlights

- The time when PER protein arrives at the perinucleus is wide and keeps changing.
- A bistable phosphoswitch enables precise nuclear entry of PER protein.
- This leads to robust circadian rhythms when cell congestion level and size change.
- This describes how the circadian clock compensates for spatiotemporal noise.

Summary

The mammalian circadian (~24h) clock is based on a self-sustaining transcriptional-translational negative feedback loop (TTFL) centered around the PERIOD protein (PER), which is translated in the cytoplasm and then enters the nucleus to repress its own transcription at the right time of day. How such precise nucleus entry, critical for generating circadian rhythms, occurs is mysterious because thousands of PER molecules transit through crowded cytoplasm and arrive at the perinucleus across several hours. Here, we investigate this by developing a mathematical model that effectively describes the complex spatiotemporal dynamics of PER as a single random time delay. We find that the spatially coordinated bistable phosphoswitch of PER, which triggers the phosphorylation of accumulated PER at the perinucleus, can lead to the synchronous and precise nuclear entry of PER, and thus to precise transcriptional repression despite the heterogenous PER arrival times at the perinucleus. In particular, even when cell crowdedness, cell size, and transcriptional activator level change, and thus PER arrival times at the perinucleus are greatly perturbed, the bistable phosphoswitch allows the TTFL to maintain robust circadian rhythms. These results provide fundamental insight into how the circadian clock compensates for spatiotemporal noise from various intracellular sources.

Introduction

The mammalian circadian (~24h) clock is a self-sustained endogenous oscillator that relies on a transcriptional-translational negative feedback loop (TTFL), where the activator complex, BMAL1:CLOCK, promotes the transcription of *Per1/2* and *Cry1/2*

49 genes, and the PER:CRY complex inhibits BMAL1:CLOCK to close the loop[1-6]. In the
50 TTFL, precise transcriptional repression (i.e., transcription being repressed at the right
51 time of the day) of BMAL1:CLOCK by the PER complex is essential to generate circadian
52 rhythms[7-10].

53 However, obtaining such precise transcriptional repression is challenging because
54 individual PER molecules are expected to arrive at the perinucleus at different times.
55 Specifically, thousands of PER molecules transit through the crowded intracellular
56 environment with organelles and macromolecules, leading to different travel times for
57 each PER molecule. Moreover, since the cell size keeps changing due to cell growth and
58 cell division, the travel distance of PER molecules to the perinucleus also keeps changing.
59 The heterogeneity in the PER arrival time is further amplified as PER molecules are
60 translated across several hours at different places[8,11,12]. Furthermore, the amount of
61 activator proteins of the transcription (e.g., BMAL1), which promotes the production of
62 PER protein, also exhibits a noisy fluctuation with daily changes[13,14]. As a result, the
63 arrival time of PER molecules largely varies during a single day and exhibits daily
64 variations. Interestingly, although thousands of PER molecules arrive at the perinucleus
65 across several hours, they enter the nucleus during a narrow time window at the right
66 time every day[8], leading to transcriptional repression with precise timing, and thus to
67 robust circadian rhythms. This indicates the existence of some mechanism that filters the
68 heterogeneity in the protein arrival time.

69 This filtering mechanism has barely been investigated. Even the widely used
70 mathematical models of the circadian clock assume that PER is homogenously
71 distributed in the cytoplasm, and thus they are not able to capture the cytoplasmic

72 trafficking of PER[15-31]. Notably, it has been shown that when the cytoplasmic trafficking
73 of Hes1 molecules is incorporated into a mathematical model, the period of Hes1
74 oscillation greatly changes (~three-fold)[32]. This indicates that the variability in the protein
75 arrival time distribution should be filtered to generate stable rhythms. Previously, a
76 potential filtering mechanism was proposed: If traveling molecules degrade quickly
77 enough, molecules that spend a long time during cytoplasmic trafficking are degraded
78 before they arrive at the perinucleus[33], and thus only molecules traveling along optimal
79 paths enter the nucleus without being degraded. Although this results in a narrow
80 distribution of nuclear entry time, it requires an unrealistically short half-life of proteins (on
81 the order of 1ms)[34]. Recently, a biologically feasible filtering mechanism, the spatially
82 coordinated bistable phosphoswitch of PER, was suggested[8]. That is, when enough PER
83 molecules are accumulated in the perinucleus, the bistable switch-like phosphorylation of
84 PER is triggered. As a result, PER molecules at the perinucleus are synchronously
85 phosphorylated, which is necessary for their nuclear entry, and enter the nucleus together.
86 This allows thousands of PER molecules that arrive at the perinucleus at different times
87 to enter the nucleus within a narrow time window. However, such filtering effect was
88 investigated only under an ideal condition that does not include critical factors that affect
89 the protein arrival time, such as variation in cytoplasmic congestion level, cell size, and
90 activator amount.

91 Here, we investigated whether the bistable phosphoswitch of PER can filter the
92 variability in its arrival time distribution under various noise sources: different cytoplasmic
93 congestion levels, cell sizes, and activator amounts. Specifically, we developed a
94 stochastic model simulating the TTFL of PER, where the PER travel time to the

perinucleus is described by a time delay distribution. Thus, changing the delay parameters allows us to effectively describe the change in the travel time due to the variation in cytoplasmic congestion and cell size. Using the framework, we found that the bistable phosphorylation of PER can effectively filter the heterogeneity in PER arrival time, resulting in precise repression timing and robust circadian rhythms. On the other hand, such filtering does not occur when PER phosphorylation occurs via conventional phosphorylation mechanisms, such as linear and ultrasensitive phosphorylations. Furthermore, by integrating our model with a previously measured BMAL1 time series in a single cell[14], we showed that the bistable phosphorylation can lead to the precise timing of nuclear entry and robust circadian rhythms even under the large intra- and inter-daily variation in the amount of the activator proteins. Taken together, the bistable phosphoswitch for nuclear entry can filter heterogeneity in protein arrival time and lead to robust rhythms under diverse environments. Our approach sets the stage for systematically exploring how the circadian clock can filter diverse spatiotemporally generated noises in the cell to generate robust circadian rhythms.

Results

Synchronous nuclear entry of PER molecules compensates for their spatiotemporal heterogeneity and leads to robust circadian rhythms.

In the TTFL of the mammalian circadian clock, the translated PER protein at the cytoplasm (R_c) approaches the perinucleus while it forms a complex with CRY proteins and CK1δ/ε (R_p), and it is phosphorylated at multiple sites (Figure 1A)[35-39]. Then, the phosphorylated PER complex in the perinucleus (R_p') can enter the nucleus, where the

PER complex (R_n) represses its own transcriptional activator (A). As R_c transits through the cytoplasm crowded with organelles and macromolecules (Figure 1A, blue circles)[8,11,12,40,41], the time R_c spends traveling to the perinucleus (τ) greatly differs, and thus the distribution of its arrival time at the perinucleus (t_p) is wide (Figure 1B (i)). The distribution of t_p becomes even wider because PER proteins are translated at different places in the cytoplasm over several hours, leading to different travel distances and departure times, respectively[8,11,12]. Thus, if R_p' enters the nucleus in the order of arrival at the perinucleus, nuclear entry occurs within a wide time window (i.e., the distribution of t_n is wide) (Figure 1B (ii), green), and thus transcriptional activity decreases gradually (Figure 1B (iii), green), weakening the circadian rhythms (Figure 1B (iv), green)[42-44]. Thus, to generate strong circadian rhythms, a mechanism narrowing the distribution of t_n is required (Figure 1B, red). Such a mechanism is expected to be based on the phosphorylation mechanism of R_p because R_p can enter the nucleus after phosphorylation[3,35,45].

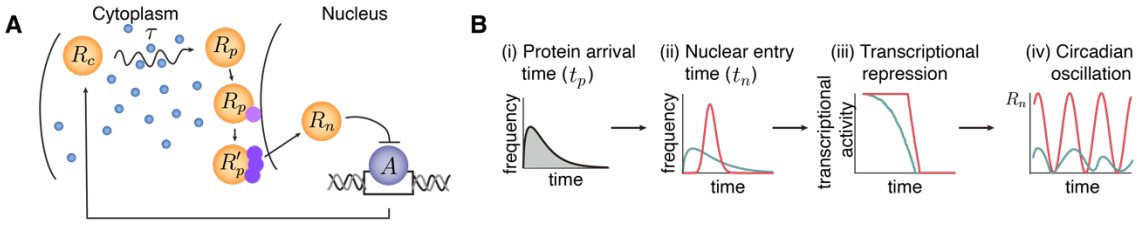

Figure 1. Precise timing of repression is required to generate robust circadian rhythms. (A) Schematic diagram of the circadian clock model. PER protein is synthesized in the cytoplasm (R_c) and then it transits toward the perinucleus while it forms a complex with CRY and CK1δ/ε (R_p), and it undergoes multisite phosphorylation. After being phosphorylated, PER complex in the perinucleus (R_p') can enter the nucleus (R_n) to

inhibit its own transcriptional activator (A). As R_c passes through cytoplasm crowded with obstacles such as organelles (blue circles), the time spent during the transit (τ) is heterogeneous among individual molecules. **(B)** This leads to a wide distribution of arrival time at the perinucleus (t_p) of the PER proteins (i). Without a filtering mechanism, the distribution of nuclear entry time (t_n) also becomes wide (green line, (ii)), leading to a gradual decline of transcriptional activity (green line, (iii)), and thus weak circadian rhythms (green line, (iv)). A filtering mechanism narrowing the distribution of t_n (red line, (ii)) is needed for sharp transcriptional repression (red line, (iii)), and thus robust circadian rhythms (red line, (iv)).

Bistable phosphorylation of PER is required to enter the nucleus in the circadian clock.

PER protein has multiple CK1-dependent phosphorylation sites where the phosphorylation of these sites occurs in a cooperative manner[8,46]. As a result, the phosphorylation occurs collectively, i.e., the phosphorylation is affected by the local concentration of the PER complex (Figure 2A, red)[8]. Specifically, when the local concentration of the PER complex is lower than the switch-on threshold (Figure 2A, black triangle), phosphorylation does not occur. However, once the local concentration reaches the switch-on threshold, the majority of the PER complex is synchronously phosphorylated, resulting in a sharp increase in the phosphorylated fraction. Furthermore, the high fraction of phosphorylated PER complex persists for awhile, even after the local concentration decreases below the switch-on threshold, until it reaches the switch-off threshold (Figure 2A, gray triangle). To investigate the advantage of having such bistable phosphorylation of R_p in reducing the heterogeneity in the distribution of t_n, we compare it with the other typical phosphorylation mechanisms: ultrasensitive phosphorylation and linear phosphorylation. Ultrasensitive phosphorylation also has a switch-on threshold for synchronous phosphorylation, similar to bistable phosphorylation, but it does not have a

distinct switch-off threshold (Figure 2A, blue)[44,47]. Thus, the fraction of the R'_p monotonically increases as the total amount of PER in the perinucleus increases, with the sigmoidal pattern having a steep increase near the switch-on threshold. In linear phosphorylation, the fraction of the R'_p is constant (Figure 2A, green): only the fixed portion of the PER complex is phosphorylated regardless of the local concentration of PER complex.

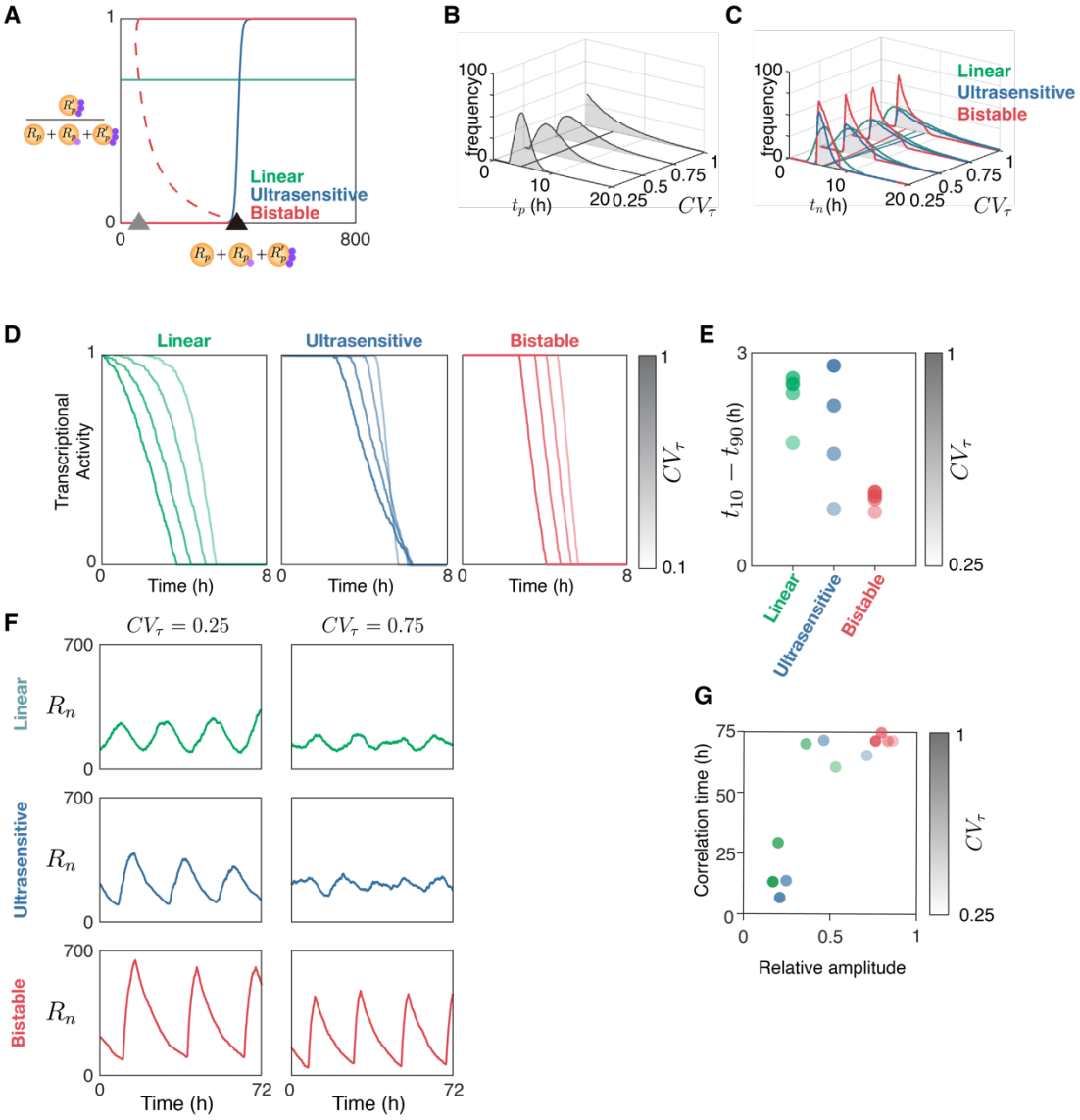

Figure 2. Spatially coordinated collective phosphorylation of PER proteins leads to robust circadian oscillations in congested cells. (A) Three representative phosphorylation mechanisms for nuclear entry. In linear phosphorylation, the fraction of R_p' is the same regardless of the local concentration of the total PER complex in the perinucleus. In ultrasensitive and bistable phosphorylations, the fraction of R_p' steeply increases when the local concentration of the total PER complex reaches the switch-on threshold (black triangle). With bistable phosphorylation, the fraction of R_p' persists even when the local concentration of the total PER complex decreases below the switch-on threshold until the local concentration of the total PER complex reaches the switch-off threshold (gray triangle). **(B-C)** As the intracellular environment becomes more crowded (i.e., CV_τ increases), thousands of PER molecules arrive at the perinucleus within a wide time window (t_p). As a result, the distribution of nuclear entry time (t_n) also becomes significantly wider with linear (green) or ultrasensitive (blue) phosphorylation, but not with bistable phosphorylation (red). Here, the distributions were obtained from 200 repeated simulations. **(D)** As CV_τ increases (light to dark colors), with linear and ultrasensitive phosphorylations, transcriptional activity decreases gradually (green and blue). In contrast, with bistable phosphorylation, transcriptional activity decreases sharply regardless of CV_τ (red). **(E)** The sensitivity of transcription repression is quantified by measuring the time taken for the transcriptional activity to decrease from 90% (t_{90}) to 10% of the maximal transcriptional activity (t_{10}). The smaller value of $t_{10} - t_{90}$ indicates the sharper repression of transcription. **(F)** Robust oscillations are maintained with bistable phosphorylation even under noisy cytoplasmic trafficking (i.e., high CV_τ), but not with linear and ultrasensitive phosphorylations. **(G)** The robustness of the oscillations was quantified by the correlation time and the relative amplitude of R_n oscillatory time series. The longer correlation time indicates the more robust oscillation.

Bistable phosphorylation of PER allows sharp transcriptional repression despite the heterogeneous PER arrival times at the perinucleus.

To investigate whether bistable phosphorylation can filter the heterogeneity in the protein arrival time (t_p), we constructed a mathematical model which describes part of the TTFL (Figure 1A): the cytoplasmic trafficking of R_c to R_p, the phosphorylation of R_p to R_p', and the nuclear entry of R_p' to R_n (see STAR Methods for detailed model descriptions and Table S1 for the propensity functions of reactions). To focus on how phosphorylation affects the distribution of t_n, we assumed that PER molecules are not degraded.

Furthermore, since directly simulating spatiotemporal dynamics during the cytoplasmic trafficking of thousands of PER molecules is computationally intractable, we describe the process with a distributed time delay (τ)[48-51]. This time delay τ is assumed to be gamma-distributed, which is similar to the distribution of time spent during the cytoplasmic trafficking of proteins[33]. Note that we used the distributed time delay rather than a fixed time delay to capture the heterogeneity in the cytoplasmic trafficking of R_c to R_p. After the arrival at the perinucleus, R_p undergoes phosphorylation with one of the three phosphorylation mechanisms (Figure 2A) and enters the nucleus. To describe these different types of phosphorylation, we adopted the modular approach, which describes complex multistep reactions with a single phenomenological module that qualitatively describes the dynamical behavior[47,52]. This allowed us to simulate the complex phosphorylation process, which is a necessary step for nuclear entry (see STAR Methods). We simulated the situation where 1,000 PER complexes travel from the cell membrane to the perinucleus using the delayed Gillespie algorithm[53,54]. This allowed us to calculate the time when each R_c arrives at the perinucleus (t_p) and then when it enters the nucleus (t_n). In this way, we obtained the distribution of t_p and t_n of the 1,000 PER complexes, which quantifies the heterogeneity in the protein arrival time and the nuclear entry time, respectively.

The cytoplasm in which R_c diffuses can become overcrowded due to various reasons, such as increased fat deposition, hindering the cytoplasmic trafficking[8-10]. This leads to noisier cytoplasmic trafficking of PER molecules, and thus they arrive at the perinucleus in a wider time window. That is, as the coefficient of variation of τ (CV_τ) increases, the distribution of t_p becomes wider (Figure 2B). As a result, the distribution of

t_n also becomes wider with linear and ultrasensitive phosphorylations (Figure 2C, green and blue), and thus transcriptional activity decreases gradually (Figure 2D, green and blue). However, the narrow distribution of t_n is maintained with bistable phosphorylation (Figure 2C, red), and thus transcriptional repression occurs sharply regardless of the CV_τ (Figure 2D, red). To quantify the sensitivity of the transcriptional repression (i.e., how rapidly the transcriptional activity is decreased), the difference between the time when the transcriptional activity reaches 10% of the maximal transcriptional activity (t_{10}) and the time when the transcriptional activity reaches 90% of the maximal transcriptional activity (t_{90}) was calculated. With bistable phosphorylation, $t_{10} - t_{90}$ is small (i.e., sharp repression) regardless of CV_τ (Figure 2E). On the other hand, with linear and ultrasensitive phosphorylations, $t_{10} - t_{90}$ greatly increases as CV_τ increases. This indicates that bistable phosphorylation, but not linear and ultrasensitive phosphorylations, allows sharp transcriptional repression even when the cytoplasmic trafficking becomes noisy.

Bistable phosphorylation generates robust circadian rhythms even with cytoplasmic congestion.

In the previous section, to focus on the cytoplasmic trafficking of R_c, we used a model describing part of the TTFL (Figure 1A). Now, we have extended the model to fully describe the TTFL. Specifically, in the model, the transcriptional activator (A) is suppressed by R_n via protein sequestration[19,21,22,28], which closes the negative feedback loop. Furthermore, the degradations of R_c, R_p, R_p', and R_n were also incorporated into the model. With this model, we investigated how the noise level in the cytoplasmic trafficking

(i.e., CV_τ) affects circadian rhythms. As CV_τ increases, the simulated oscillations of R_n become noisy with linear and ultrasensitive phosphorylations (Figure 2F, green and blue). On the other hand, even when CV_τ increases, robust oscillations are maintained with bistable phosphorylation (Figure 2F, red). To quantify the accuracy and the strength of the simulated oscillations, we calculated the correlation time and the relative amplitude of the time series of R_n (see STAR Methods). The correlation time describes how fast the autocorrelation function of the oscillatory time series decays[55,56]. If the time series exhibits a noisy oscillation, autocorrelation will decay rapidly, resulting in a short correlation time. The correlation time becomes short and relative amplitude becomes small with linear and ultrasensitive phosphorylations when CV_τ increases (Figure 2G, green and blue). On the other hand, the correlation time is long and the relative amplitude is large regardless of CV_τ with bistable phosphorylation (Figure 2G, red). Taken together, with bistable phosphorylation, robust oscillations can be generated even when CV_τ is large due to noisy cytoplasmic trafficking.

Bistable phosphorylation reduces the effect of cell size variation on circadian periods.

Next, we investigated the effect of cell size variation, which is another source leading to the variation in the distribution of τ, on circadian rhythms. Specifically, mouse fibroblast cells have highly variable areas (mean $\pm$ SD, $2346 \pm 558\ \mu m^2$; CV=24%) (Figure 3A (i))[57]. Such cell size variation varies the distance of the cytoplasmic trafficking, and thus it is expected that the mean (μ_τ) and standard deviation (σ_τ) of τ changes depending on the cell size. To explore this, we used a partial differential equation (PDE) that

describes the cytoplasmic trafficking of molecules via diffusion toward the perinucleus by adopting the approach used in a previous study[33](see Supplemental Information for details). By simulating the PDE with an experimentally measured diffusion coefficient of PER molecules ($D = 0.2\mu m^2/s$)[11,12] and cell sizes[57], we obtained the probability of having a PER molecule at each distance from the nucleus and each time. This allowed us to obtain the probability distribution of the PER arrival time at the perinucleus. In particular, we found that the mean ± SD of μ_τ and σ_τ are 5.04 ± 1.91h and 4.95 ± 1.89 h, respectively (Figure 3A (ii), when cell size varies according to $N(2346\mu m^2,\ 558^2\mu m^4)$ (Figure 3A (i)) (see STAR Methods). Unexpectedly, the standard deviations of both μ_τ and σ_τ are ~2h, which is about double of the standard deviation of the circadian periods of the mouse fibroblast cells with different sizes (mean ± SD, 22.97 ± 0.91h) (Figure 3A (ii))[57]. This indicates the presence of filtering mechanisms for the heterogeneous cytoplasmic trafficking time (τ) to generate similar circadian periods across different cell sizes.

To investigate whether bistable phosphorylation can compensate for the effect of cell size variation, we simulated the TTFL model used in Figures 2F and 2G for cells with different sizes. Specifically, we varied μ_τ according to $N(5.04\text{h}, 1.91^2\text{h}^2)$, whose mean and SD are obtained from Figure 3A (ii). Furthermore, we set $\sigma_\tau = 0.5 \times \mu_\tau$, about half of those obtained from the PDE simulation ($\sigma_\tau \approx \mu_\tau$), because $\sigma_\tau \approx \mu_\tau$ leads to too noisy rhythms with linear and ultrasensitive phosphorylations to analyze their periods and amplitudes (Figure 2G). As μ_τ and σ_τ vary due to the cell size change, bistable phosphorylation leads to a much narrower distribution of periods (SD=2.20h) compared to linear and ultrasensitive phosphorylations (SD=4.28h and SD=4.31h, respectively)

(Figure 3B). Thus, bistable phosphorylation reduces the effect of cell size variation on the circadian period.

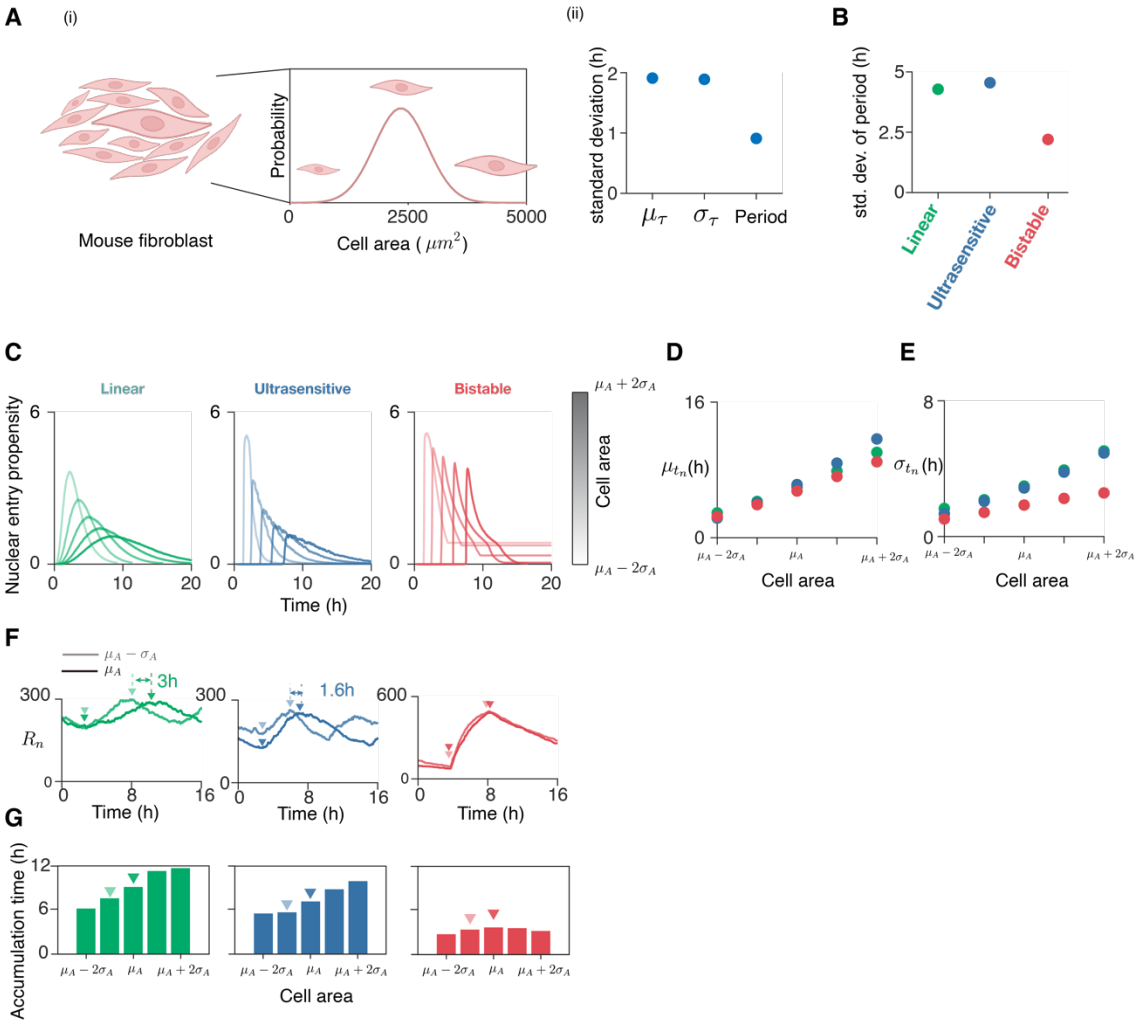

Figure 3. Bistable phosphorylation enables cells of different sizes to have similar periods. (A) (i) Mouse fibroblast cell size is highly variable, having mean ± SD, 2346 ± 558 μm^2 (CV=24%)[57]. (ii) For mouse fibroblast cells with different sizes, although the standard deviation of the mean (μ_τ) and the standard deviation (σ_τ) of time spent during the cytoplasmic trafficking are ~2h, the standard deviation of the circadian periods is only a half of them (SD=0.91h). **(B)** The standard deviation of the simulated circadian periods for 1,000 cells, whose areas were sampled from the $N(2346\mu m^2,\ 558^2\mu m^4)$. **(C)** In a larger cell, μ_τ and σ_τ increase. Thus, the time trajectories of the nuclear entry propensity (Tables S1 and S2) are shifted to the right and become wider. Note that with bistable phosphorylation, the nuclear entry occurs in a narrow time window, even in larger cells. The distributions were obtained with 200 repeated simulations. μ_A (=2346μm^2) and σ_A

(=558μm^2) are the mean and standard deviation of fibroblast cell area, respectively. **(D-E)** While the mean of the nuclear entry time (μ_{t_n}) increases similarly in all three phosphorylation mechanisms, bistable phosphorylation resulted in a far smaller standard deviation in nuclear entry time (σ_{t_n}) than linear and ultrasensitive phosphorylations. **(F-G)** As a result, the length of time during which R_n accumulates from the trough (triangle) to the peak (triangle) of R_n does not change regardless of cell area with bistable phosphorylation, but this is not the case with linear and ultrasensitive phosphorylations.

Bistable phosphorylation mitigates the slowed nuclear entry when cell size increases.

We investigated how bistable phosphorylation compensates for the effect of cell size changes on the circadian period. For this, we used a model describing part of the TTFL (Figures 2B and 2C) for the five representative cell areas: $\mu_A - 2\sigma_A$, $\mu_A - \sigma_A$, μ_A, $\mu_A + \sigma_A$, and $\mu_A + 2\sigma_A$, where μ_A (=2346μm^2) and σ_A (=558μm^2) are the mean and standard deviation of areas of fibroblast cells, respectively (Figure 3A(i)). As the cell size increases, and thus μ_τ increases, the simulated time trajectories of the nuclear entry propensity (Tables S1 and S2) are shifted to the right (Figure 3C). Thus, the mean of nucleus entry time (t_n) increases for all three phosphorylation mechanisms (Figure 3D), which is expected to lengthen the period. Furthermore, as σ_τ also increases due to the cell size increase, PER molecules enter the nucleus in a wider time window, and thus the time trajectories of the nuclear entry propensity become wider and lower. Lower nuclear entry propensity results in a slow increase in R_n (Figure 3C), which may further lengthen the period. Interestingly, such change is much smaller with bistable phosphorylation compared to linear and ultrasensitive phosphorylation (Figure 3C). That is, the increase in the standard deviation of t_n is significantly larger with linear and ultrasensitive phosphorylations than with bistable phosphorylation (Figure 3E). As a result, when the

TTFL model was simulated for each phosphorylation mechanism, the time between the minimum of R_n and the maximum of R_n became longer (i.e., R_n accumulated more slowly) in a larger cell with linear and ultrasensitive phosphorylations, but not with bistable phosphorylation (Figure 3F). Specifically, the mean length of time during which R_n increased more than two-fold change varied from ~4h to ~10h as the cell area increased from $\mu_A - 2\sigma_A$ (=1229 μm^2) to $\mu_A + 2\sigma_A$ (=3462 μm^2) with linear and ultrasensitive phosphorylations (Figure 3G, green and blue). On the other hand, with bistable phosphorylation, the accumulation time of R_n was nearly the same regardless of the cell area (Figure 3G, red). This explains why the change in the circadian period due to the cell size variation is smaller with bistable phosphorylation than with other phosphorylation mechanisms (Figure 3B).

Bistable phosphorylation enables robust circadian rhythms despite noisy activator rhythms.

In the previous sections, the amount of activator protein was assumed to be constant over time. However, the amount of activator molecules, such as BMAL1, oscillates with a period of ~24h[13,14,35,58] (Figure 4A). In addition, the amplitude and the peak-to-peak period of BMAL1 protein fluctuate from day to day. Specifically, the amplitude and the peak-to-peak period of experimentally measured BMAL1 proteins in a single cell highly vary[14]: 286±35 and 25.4±5.7h (Figure 4A). Furthermore, an additional 'bump' often exists between the peaks. Due to the noisy pattern, it is expected that the synthesis timing of PER will be heterogeneous, resulting in the heterogeneous protein arrival time distribution. We investigated whether bistable phosphorylation enables robust

circadian rhythms of PER even under such fluctuation in activators, resulting in noisy transcription of PER. For this, we simulated the TTFL model (Figure 1A), where the activator level changes according to the experimentally measured BMAL1 (Figure 4A). The amplitude of oscillation is highly variable with linear and ultrasensitive phosphorylations (Figure 4B, green and blue). Furthermore, additional peaks in the nuclear PER complex (R_n) are observed with linear and ultrasensitive phosphorylations. In contrast, with bistable phosphorylation, robust rhythms with similar amplitudes are generated (Figure 4B, red). Moreover, the additional peaks do not appear. As a result, the CV of the peak-to-peak period and the amplitude are much smaller with bistable phosphorylation than with linear and ultrasensitive phosphorylations (Figure 4C). Taken together, bistable phosphorylation enables robust circadian rhythms despite fluctuation in activator rhythms.

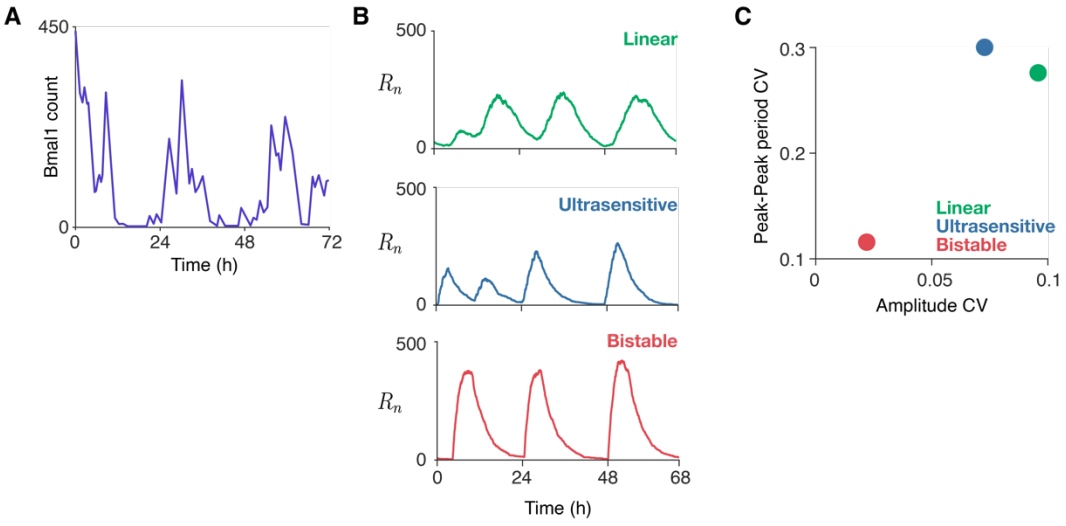

Figure 4. Bistable phosphorylation enables cells to sustain robust circadian rhythms even under noisy activator rhythms. (A) The level of activator protein BMAL1 fluctuates across a day and exhibits daily change. In addition, an additional bump often exists, resulting in more than one peak during a single cycle. The graph was retrieved

from Blanchoud et al.[14]. **(B)** Even with such noisy activator time series, bistable phosphorylation leads to robust rhythms, unlike linear and ultrasensitive phosphorylations. **(C)** As a result, the CV of both the peak-to-peak period and the amplitudes is small with bistable phosphorylation, but not with linear and ultrasensitive phosphorylation.

Discussion

For the TTFL to generate robust circadian rhythms, precise nucleus entry of the PER complex is critical[7-10]. However, the distribution of the PER complex arrival time at the perinuclear region is highly heterogeneous due to various noise sources. Despite this, precise nucleus entry of the PER complex and transcriptional repression occur in the circadian clock. To investigate the molecular mechanism underlying the unexpected precision of the circadian clock, we constructed a mathematical model describing the effect of protein arrival time on circadian rhythms (Figure 1A). We found that when the protein arrival time varies due to the change of cytoplasmic congestion level, cell size, and activator level, bistable phosphorylation, but not linear and ultrasensitive phosphorylations, leads to precise repression timing, and thus robust circadian rhythms (Figures 2-4). This indicates that the bistable phosphoswitch is the key mechanism to filter the spatiotemporal noise in the cell to generate circadian rhythms. The spatiotemporally regulated bistable phosphorylation can also play a critical role in other biological oscillators, such as the cell cycle[59-61].

The mathematical model used in our study describes the spatiotemporal dynamics of the TTFL of the circadian clock. In previous studies, the spatiotemporal dynamics of molecules from the cytoplasm to the nucleus were directly described using PDE[33] or agent-based models[8,32]. This approach was computationally expensive and not flexible to describe the various noise sources for the protein arrival time of molecules to the

perinucleus. To describe the spatiotemporal dynamics of molecules simply and flexibly, we used a delay distribution, which was previously used to describe a chain of signaling processes or protein synthesis[48-50]. Furthermore, it is challenging to model ultrasensitive and bistable phosphorylations since they are generated from complex combinations of multiple reactions. To resolve this, we utilized a modular approach that describes those complex multistep reactions with a phenomenological module, which was developed in work by De Boeck et al.[47]. This allowed us to effectively capture the key dynamics of the phosphorylation mechanisms without comprehensively modeling the underlying complex reactions. The time delay distribution and the modular approach are effective tools for describing complex intracellular spatiotemporal dynamics.

The bistable phosphoswitch regulates the nuclear entry of PER. Specifically, it allows PER molecules to enter the nucleus after phosphorylation only when the local concentration of PER in the perinucleus reaches a certain level, rather than entering the nucleus in the order in which molecules arrive near the nucleus[8]. This type of regulation of nuclear entry could also play an important role in biological systems other than the circadian clock. For example, in pancreatic β-cells, the nuclear entry of cPKA should be slow to distinguish the time scales of external signals[62]. However, the underlying molecular mechanisms of such slow nuclear entry have not been known. The bistable phosphoswitch could be a potential molecular mechanism leading to such regulation of cPKA in pancreatic β-cells.

Alzheimer's disease (AD) has been reported to disrupt the circadian clock[63]. Such distribution appears to be due to tauopathy, which triggers the formation of neurofibrillary tangles, and thus increases cytoplasmic crowdedness[8]. However, even though tauopathy

is one of the earliest events in AD development[64], the activity rhythms of mild symptomatic dementia patients are not significantly different from those of non-patients[65,66]. This can be explained by our results: the bistable phosphoswitch allows the circadian rhythms to function normally up to a reasonable increase in intracellular congestion level.

Limitations of the study

In this work, we utilized an extension of the Gillespie algorithm to simulate the system describing the TTFL. This allowed us to describe the effects of various noise sources on circadian rhythms. To use the Gillespie algorithm for a system containing non-elementary propensity functions (e.g., Hill functions) other than functions from mass-action kinetics, timescale separation is necessary[67-69]. Thus, we assumed that the synthesis and the degradation of PER are slower than other reactions, such as binding and unbinding of PER to activator proteins and each step of its phosphorylation and dephosphorylation. However, timescale separation is often not enough for accurate stochastic simulations, unlike deterministic simulations; i.e., the condition for using the non-elementary propensity functions for stochastic simulation is stricter than the deterministic simulations[68,70-72]. Furthermore, the validity of using non-elementary propensity functions for stochastic simulations in the presence of distributed delays has not been investigated, which will be interesting in future work.

Cell size keeps changing due to cell growth or cell division, which affects the TTFL of the circadian clock. Specifically, as cell size changes, the cytoplasmic trafficking of PER molecules changes, which is investigated in our study by using a time delay distribution (Figures 3B-3G). However, we did not investigate other critical factors, such as the

449 dilution of the PER molecules during cell growth and their partition into daughter cells
450 after cell division[73-75]. It would be interesting in future work to extend our study to
451 incorporate dilution due to cell growth and the partition of molecules after cell division to
452 investigate further the effect of the cell size changes on circadian rhythms.

453

454 Acknowledgements

455 This work was supported by the Human Frontiers Science Program Organization (grant
456 no. RGY0063/2017) (J.K.K.), the Institute for Basic Science (grant no. IBS-R029-C3)
457 (J.K.K.), the Korea University Grant (S.L.) and the National Research Foundation of
458 Korea (NRF) grant funded by the Korea government (MSIP) (No.
459 2020R1A2C1A01100114) (S.L).

460

461 Author contributions

462 All authors designed the study. S.J.C. performed and D.W.K., S.L. and J.K.K. contributed
463 to computational modeling and simulation. All authors analyzed the data. J.K.K.
464 supervised the project. S.J.C. and J.K.K. wrote the draft of the manuscript, and all authors
465 revised the manuscript.

466

467 Declaration of interests

468 The authors declare no competing interests.

469

470 STAR★Methods

RESOURCE AVAILABILITY

Lead contact

Further information and requests for resources and reagents should be directed to and will be fulfilled by the Lead Contact, Jae Kyoung Kim (jaekkim@kaist.ac.kr).

Materials availability

This study did not generate new unique reagents.

Data and code availability

- This paper analyzes publicly available existing data. These accession numbers for the datasets are listed in the key resources table.
- The MATLAB codes of the computational package are available in the following Database: The link will be available upon acceptance of the manuscript.
- Any additional information required to analyze the data is available from the lead contact upon request.

METHODS DETAILS

The stochastic model of the circadian clock simulating the TTFL with the spatiotemporal behavior of PER proteins.

We extended a previous mathematical model of the mammalian circadian clock[19,21,22,28] to study the influence of the spatiotemporal behavior of PER proteins on circadian rhythms (see Tables S1 and S2 for detailed reactions and parameters used in the simulation). Specifically, our model consists of four variables: PER protein in the peripheral cytoplasm (R_c), unphosphorylated PER complex in the perinucleus (R_p),

phosphorylated PER complex in the perinucleus (R_p'), and PER complex in the nucleus (R_n), which degrade with the same rate constant of λ_d.

In the model, R_c is synthesized at the rate of $\lambda_p \max\left(1-\frac{R_n}{A}, 0\right)$, where A is the number of activator proteins and λ_p is the maximum synthesis rate. The synthesis rate is proportional to the fraction of free activator that is not sequestrated by PER complex in the nucleus, described by $\max\left(1-\frac{R_n}{A}, 0\right)$. This is an approximated form of the quasi-steady state of the fraction of free activators found by applying the total quasi-steady state approximation reduction to the detailed model describing the circadian clock[19,21,22,28] under the assumption that PER quickly binds and unbinds to the activator: $\frac{A-R_n-K_d\Omega+\sqrt{(A-R_n-K_d\Omega)^2+4AK_d\Omega}}{2A}$, where K_d is the dissociation constant between the activator and PER, and Ω is the volume of the system. Then, by further assuming that the binding is tight ($K_d \to 0$), the fraction of free activator can be approximated by $\max(1-\frac{R_n}{A}, 0)$[19,21,22,28]. Up to Figure 3, A was fixed to be 300, assuming the number of the activator is constant over time to focus on the spatiotemporal dynamics of PER. In Figure 4, to investigate whether bistable phosphorylation enables robust circadian rhythms even under noisy activator rhythms, we changed A according to the experimentally measured time series of BMAL1 molecules in a single cell[14]. From 72h-long experimentally measured BMAL1 data, the first four hours were excluded to avoid the effect of the initial shock for the experiment and then repeated to generate a long time series of A. Since the experimentally measured BMAL1 time series was discrete, we linearly interpolated the data to obtain the amount of BMAL1 in continuous time.

After being synthesized, R_c passes through the cytoplasm crowded with obstacles during a gamma-distributed time delay τ. Specifically, when each R_c molecule is produced, τ is sampled from the gamma distribution and assigned to each molecule. Here, the gamma distribution is utilized because it successfully captures the distribution of time spent during the cytoplasmic trafficking[33]. To determine the shape of the gamma distribution, we utilized a previously proposed method using the PDE model, which describes the cytoplasmic trafficking[33], so that the mean and the standard deviation of τ can be obtained (see Supplemental Information for details). When the experimentally measured diffusion coefficient of PER of $0.2\mu m^2/s$[11,12] and the mean area of the fibroblast cell of $2346\mu m^2$ were used, the PDE simulation resulted in μ_τ=4.9h. This value of μ_τ was used in Figure 2 and Figure 4. σ_τ was set to be $\sigma_\tau = 0.5 \cdot \mu_\tau$ to ensure linear and ultrasensitive phosphorylations to generate oscillations.

The PER complex that arrives at the perinucleus (R_p) undergoes phosphorylation to be R_p'. Then, R_p' is either dephosphorylated to R_p with the rate of $\frac{1}{\tau_p}$ or enters the nucleus with the rate of λ_n. To simply describe the phosphorylation based on multiple reactions, we adopted the modular approach[47], which treated the phosphorylation reaction as a single phenomenological module. That is, the module takes the total amount of PER complex in the perinucleus ($T = R_p + R_p'$) as the input and gives the fraction of the R_p' in the perinucleus as the output. Among possible responses that the module can generate, we chose linear phosphorylation, ultrasensitive phosphorylation, and bistable phosphorylation[52]. With linear phosphorylation, the fraction of R_p' ($=\frac{R_p'}{T}$) is constant regardless of T (Figure 2A, green). Such response is obtained by utilizing the propensity

function for the phosphorylation $f(T) = \frac{c \cdot T}{\tau_p}$, where c is between 0 and 1. In our simulation, the time scale of phosphorylation and dephosphorylation reactions, τ_p, was set to be sufficiently short ($\tau_p = \frac{1}{60}$h) so that the phosphorylation and dephosphorylation quickly equilibrate (i.e., $\frac{c \cdot T}{\tau_p} = \frac{R_p'}{\tau_p}$). As a result, the fraction of R_p' equilibrates to $\frac{R_p'}{T} = c$. Here, $c = 0.7$ was chosen to make the fraction of R_p' be 70%. For ultrasensitive phosphorylation, the fraction of R_p' monotonically increases as T increases, with a steep increase near the threshold. To describe ultrasensitive phosphorylation, the propensity function $f(T) = \frac{1}{\tau_p}\left(\frac{T^{n+1}}{T^n + K_u^n}\right)$ was used. Thus, the fraction of R_p' ($\frac{R_p{}'}{T}$) quickly equilibrates to $\frac{T^n}{T^n + K_u^n}$, which was used to describe the ultrasensitive response previously[44,47]. We set $K_u = 400$ and $n = 70$ to obtain a steep increase in the fraction of R_p' when T reaches 400 (Figure 2A, blue). For bistable phosphorylation, the response is bifurcating (i.e., the response qualitatively varies depending on variables other than T), being affected by R_p'. Thus, the response of bistable phosphorylation is described not only by T, but also by R_p'. To describe bistable phosphorylation, we used an implicit function $f(T, R_p') = \frac{1}{\tau_p}\left(\frac{T^{m+1}}{T^m + \max(0.125 \cdot K_b, K_b - 5 \cdot R_p')^m}\right)$ after modifying a function generating an S-shaped response curve (i.e., bistable response)[47]. $\frac{R_p'}{T}$ quickly equilibrates to $\frac{T^m}{T^m + \max(0.125 \cdot K_b, K_b - 5 \cdot R_p')^m}$, which steeply increases when T increases to reach the switch-on threshold, K_b. Once T reaches K_b, the fraction of R_p' stays near one even though T decreases below K_b until it reaches the switch-off threshold, which is about $\frac{K_b}{8}$. Here, we chose $m = 30$ and $K_b = 400$ (Figure 2A, red).

555 The model was simulated using the delayed Gillespie algorithm[53,54]. For the
556 Gillespie simulation, the volume of the system was set to 1. See Tables S1 and S2 for
557 detailed descriptions of propensity functions and parameters used in the simulation,
558 respectively. In Figures 2B-2E and Figures 3C-3E, to focus on how the phosphorylation
559 affects the distribution of t_n, the synthesis of R_c and the degradation of PER molecules
560 are excluded from the simulation. Specifically, we set λ_p and λ_d to be 0 to make these
561 reactions not occur. The initial condition was given by $R_c = 1000$, $R_p = R_p' = R_n = 0$.
562

563 ## QUANTIFICATIONS AND STATISTICAL ANALYSIS

564 **Quantification of features of the oscillation.**

565 We calculated several features (e.g., period, amplitude, correlation time) from the
566 oscillatory time series. First, in Figure 2G, we calculated the correlation time[55,56] and the
567 relative amplitude[31], as done in previous studies. Specifically, to calculate the correlation
568 time, we estimated parameters τ_C and P by fitting $DC(s) = \exp\left(-\frac{s}{\tau_C}\right) \cdot \cos\left(\frac{2\pi s}{P}\right)$ to the
569 autocorrelation function $C(s) = \frac{\langle (x(t+s)-\langle x\rangle)(x(t)-\langle x\rangle)\rangle_s}{\langle x^2\rangle - \langle x\rangle^2}$ where $x(t)$ is the R_n time series
570 obtained from the simulation. Then, the correlation time is defined as τ_C, and it describes
571 how fast the autocorrelation decays over time. Thus, a more robust oscillation has a larger
572 τ_C. The relative amplitude was calculated as the fraction of the amplitude (i.e., the
573 difference between the peak height and trough height of the given rhythms) to the peak
574 height. To calculate the correlation time and the relative amplitude, the R_n time series
575 obtained from the simulation for 100 days (i.e., 2,400h) was used after the first 10 days
576 were excluded to avoid the effect of transient dynamics. We repeated ten simulations with

the same initial condition of having no PER molecule in the cell. Then, we took the average correlation time over ten repetitions.

In Figure 3B, we calculated the period of the oscillation by fitting the $C(s)$ to $DC(s)$ for simulated time series of R_n for 100 days after excluding first 10 transient days. Then, we used the estimated P as the period. We repeated this over ten different simulated trajectories and used the average of the estimated P as the period.

To calculate the accumulation time of R_n in Figure 3G and the peak-to-peak period in Figure 4, the time series of R_n simulated for 100 days after excluding first 10 transient days was used. Then, the accumulation time of R_n was measured from each cycle over 10 repeated simulations and then the mean of R_n accumulation time was calculated. The peak-to-peak period was measured from each cycle over 10 repeated simulations, and then CV was calculated (Figure 4).

KEY RESOURCE TABLE

REAGENT or RESOURCE	SOURCE	IDENTIFIER
Software and algorithms		
MATLAB R2021b	MathWorks	https://mathworks.com; RRID:SCR_001622
Others		
Mouse fibroblast cell size data	Li et al.[57]	https://www.pnas.org/doi/full/10.1073/pnas.1922388117
BMAL1 time series data	Blanchoud et al.[14]	https://www.sciencedirect.com/science/article/abs/pii/S1046202315001700X

References

1. Reppert, S.M., and Weaver, D.R. (2001). Molecular analysis of mammalian circadian rhythms. Annu Rev Physiol *63*, 647-676. https://doi.org/10.1146/annurev.physiol.63.1.647.
2. Ueda, H.R., Chen, W., Adachi, A., Wakamatsu, H., Hayashi, S., Takasugi, T., Nagano, M., Nakahama, K., Suzuki, Y., Sugano, S., et al. (2002). A transcription factor response element for gene expression during circadian night. Nature *418*, 534-539. 10.1038/nature00906.
3. Gallego, M., and Virshup, D.M. (2007). Post-translational modifications regulate the ticking of the circadian clock. Nat Rev Mol Cell Biol *8*, 139-148. https://doi.org/10.1038/nrm2106.
4. Takahashi, J.S. (2017). Transcriptional architecture of the mammalian circadian clock. Nat Rev Genet *18*, 164-179. https://doi.org/10.1038/nrg.2016.150.
5. Honma, S. (2018). The mammalian circadian system: a hierarchical multi-oscillator structure for generating circadian rhythm. J Physiol Sci *68*, 207-219. https://doi.org/10.1007/s12576-018-0597-5.
6. Cao, X., Yang, Y., Selby, C.P., Liu, Z., and Sancar, A. (2021). Molecular mechanism of the repressive phase of the mammalian circadian clock. Proc Natl Acad Sci U S A *118*. https://doi.org/10.1073/pnas.2021174118.
7. Tamanini, F., Yagita, K., Okamura, H., and van der Horst, G.T.J. (2005). Nucleocytoplasmic Shuttling of Clock Proteins. In Methods in Enzymology, M.W. Young, ed. (Academic Press), pp. 418-435. https://doi.org/10.1016/S0076-6879(05)93020-6.
8. Beesley, S., Kim, D.W., D'Alessandro, M., Jin, Y., Lee, K., Joo, H., Young, Y., Tomko, R.J., Faulkner, J., Gamsby, J., et al. (2020). Wake-sleep cycles are severely disrupted by diseases affecting cytoplasmic homeostasis. Proceedings of the National Academy of Sciences *117*, 28402-28411. https://doi.org/10.1073/pnas.2003524117.
9. Hurley, J.M. (2020). Cytoplasmic traffic jams affect circadian timing. Science Translational Medicine *12*, eabf4681. https://doi.org/10.1126/scitranslmed.abf4681.
10. Montague-Cardoso, K. (2020). Sleep-wake cycles are disrupted by diseases that result in cytoplasmic crowding. Communications Biology *3*, 705. https://doi.org/10.1038/s42003-020-01445-8.
11. Smyllie, N.J., Pilorz, V., Boyd, J., Meng, Q.J., Saer, B., Chesham, J.E., Maywood, E.S., Krogager, T.P., Spiller, D.G., Boot-Handford, R., et al. (2016). Visualizing and Quantifying Intracellular Behavior and Abundance of the Core Circadian Clock Protein PERIOD2. Curr Biol *26*, 1880-1886. https://doi.org/10.1016/j.cub.2016.05.018.
12. Koch, A.A., Bagnall, J.S., Smyllie, N.J., Begley, N., Adamson, A.D., Fribourgh, J.L., Spiller, D.G., Meng, Q.-J., Partch, C.L., Strimmer, K., et al. (2022). Quantification of protein abundance and interaction defines a mechanism for operation of the circadian clock. eLife *11*, e73976. https://doi.org/10.7554/eLife.73976.
13. Suter, D.M., Molina, N., Gatfield, D., Schneider, K., Schibler, U., and Naef, F. (2011). Mammalian genes are transcribed with widely different bursting kinetics. Science *332*, 472-474. https://doi.org/10.1126/science.1198817.
14. Blanchoud, S., Nicolas, D., Zoller, B., Tidin, O., and Naef, F. (2015). CAST: An automated segmentation and tracking tool for the analysis of transcriptional kinetics from single-cell time-lapse recordings. Methods *85*, 3-11. https://doi.org/10.1016/j.ymeth.2015.04.023.
15. Goldbeter, A. (1995). A model for circadian oscillations in the Drosophila period protein (PER). Proc Biol Sci *261*, 319-324. https://doi.org/10.1098/rspb.1995.0153.

16. Tyson, J.J., Hong, C.I., Thron, C.D., and Novak, B. (1999). A simple model of circadian rhythms based on dimerization and proteolysis of PER and TIM. Biophys J *77*, 2411-2417. https://doi.org/10.1016/S0006-3495(99)77078-5.
17. Forger, D.B., and Peskin, C.S. (2003). A detailed predictive model of the mammalian circadian clock. Proc Natl Acad Sci U S A *100*, 14806-14811. https://doi.org/10.1073/pnas.2036281100.
18. Leloup, J.C., and Goldbeter, A. (2003). Toward a detailed computational model for the mammalian circadian clock. Proc Natl Acad Sci U S A *100*, 7051-7056. https://doi.org/10.1073/pnas.1132112100.
19. Kim, J.K., and Forger, D.B. (2012). A mechanism for robust circadian timekeeping via stoichiometric balance. Mol Syst Biol *8*, 630. https://doi.org/10.1038/msb.2012.62.
20. Jolley, C.C., Ukai-Tadenuma, M., Perrin, D., and Ueda, H.R. (2014). A mammalian circadian clock model incorporating daytime expression elements. Biophys J *107*, 1462-1473. 10.1016/j.bpj.2014.07.022.
21. Kim, J.K., Kilpatrick, Z.P., Bennett, M.R., and Josic, K. (2014). Molecular mechanisms that regulate the coupled period of the mammalian circadian clock. Biophys J *106*, 2071-2081. https://doi.org/10.1016/j.bpj.2014.02.039.
22. Kim, J.K. (2016). Protein sequestration versus Hill-type repression in circadian clock models. IET Syst Biol *10*, 125-135. https://doi.org/10.1049/iet-syb.2015.0090.
23. Wang, Y., Ni, X., Yan, J., and Yang, L. (2017). Modeling transcriptional co-regulation of mammalian circadian clock. Math Biosci Eng *14*, 1447-1462. https://doi.org/10.3934/mbe.2017075.
24. Abel, J.H., Chakrabarty, A., Klerman, E.B., and Doyle, F.J., 3rd (2019). Pharmaceutical-based entrainment of circadian phase via nonlinear model predictive control. Automatica (Oxf) *100*, 336-348. https://doi.org/10.1016/j.automatica.2018.11.012.
25. Del Olmo, M., Kramer, A., and Herzel, H. (2019). A Robust Model for Circadian Redox Oscillations. Int J Mol Sci *20*. https://doi.org/10.3390/ijms20092368.
26. Kim, D.W., Chang, C., Chen, X., Doran, A.C., Gaudreault, F., Wager, T., DeMarco, G.J., and Kim, J.K. (2019). Systems approach reveals photosensitivity and PER2 level as determinants of clock-modulator efficacy. Mol Syst Biol *15*, e8838. https://doi.org/10.15252/msb.20198838.
27. Breitenbach, T., Helfrich-Forster, C., and Dandekar, T. (2021). An effective model of endogenous clocks and external stimuli determining circadian rhythms. Sci Rep *11*, 16165. https://doi.org/10.1038/s41598-021-95391-y.
28. Kim, J.K. (2021). Tick, Tock, Circadian Clocks. In Case Studies in Systems Biology, P. Kraikivski, ed. (Springer International Publishing), pp. 79-94. https://doi.org/10.1007/978-3-030-67742-8_6.
29. Kim, R., and Reed, M.C. (2021). A mathematical model of circadian rhythms and dopamine. Theor Biol Med Model *18*, 8. https://doi.org/10.1186/s12976-021-00139-w.
30. Mosig, R.A., Castaneda, A.N., Deslauriers, J.C., Frazier, L.P., He, K.L., Maghzian, N., Pokharel, A., Schrier, C.T., Zhu, L., Koike, N., et al. (2021). Natural antisense transcript of Period2, Per2AS, regulates the amplitude of the mouse circadian clock. Genes Dev *35*, 899-913. https://doi.org/10.1101/gad.343541.120.
31. Jeong, E.M., Kwon, M., Cho, E., Lee, S.H., Kim, H., Kim, E.Y., and Kim, J.K. (2022). Systematic modeling-driven experiments identify distinct molecular clockworks underlying hierarchically organized pacemaker neurons. Proceedings of the National Academy of Sciences *119*, e2113403119. https://doi.org/doi:10.1073/pnas.2113403119.
32. Sturrock, M., Hellander, A., Matzavinos, A., and Chaplain, M.A. (2013). Spatial stochastic modelling of the Hes1 gene regulatory network: intrinsic noise can explain heterogeneity in embryonic stem cell differentiation. J R Soc Interface *10*, 20120988. https://doi.org/10.1098/rsif.2012.0988.

33. Ma, J., Do, M., Le Gros, M.A., Peskin, C.S., Larabell, C.A., Mori, Y., and Isaacson, S.A. (2020). Strong intracellular signal inactivation produces sharper and more robust signaling from cell membrane to nucleus. PLOS Computational Biology *16*, e1008356. https://doi.org/10.1371/journal.pcbi.1008356.
34. Chen, W., Smeekens, J.M., and Wu, R. (2016). Systematic study of the dynamics and half-lives of newly synthesized proteins in human cells. Chem Sci *7*, 1393-1400. https://doi.org/10.1039/c5sc03826j.
35. Lee, C., Etchegaray, J.P., Cagampang, F.R., Loudon, A.S., and Reppert, S.M. (2001). Posttranslational mechanisms regulate the mammalian circadian clock. Cell *107*, 855-867. https://doi.org/10.1016/s0092-8674(01)00610-9.
36. Isojima, Y., Nakajima, M., Ukai, H., Fujishima, H., Yamada, R.G., Masumoto, K.H., Kiuchi, R., Ishida, M., Ukai-Tadenuma, M., Minami, Y., et al. (2009). CKIepsilon/delta-dependent phosphorylation is a temperature-insensitive, period-determining process in the mammalian circadian clock. Proc Natl Acad Sci U S A *106*, 15744-15749. 10.1073/pnas.0908733106.
37. Zhou, M., Kim, J.K., Eng, G.W., Forger, D.B., and Virshup, D.M. (2015). A Period2 Phosphoswitch Regulates and Temperature Compensates Circadian Period. Mol Cell *60*, 77-88. https://doi.org/10.1016/j.molcel.2015.08.022.
38. Narasimamurthy, R., Hunt, S.R., Lu, Y., Fustin, J.M., Okamura, H., Partch, C.L., Forger, D.B., Kim, J.K., and Virshup, D.M. (2018). CK1delta/epsilon protein kinase primes the PER2 circadian phosphoswitch. Proc Natl Acad Sci U S A *115*, 5986-5991. https://doi.org/10.1073/pnas.1721076115.
39. Masuda, S., Narasimamurthy, R., Yoshitane, H., Kim, J.K., Fukada, Y., and Virshup, D.M. (2020). Mutation of a PER2 phosphodegron perturbs the circadian phosphoswitch. Proc Natl Acad Sci U S A *117*, 10888-10896. https://doi.org/10.1073/pnas.2000266117.
40. Gabriel, C.H., Del Olmo, M., Zehtabian, A., Jager, M., Reischl, S., van Dijk, H., Ulbricht, C., Rakhymzhan, A., Korte, T., Koller, B., et al. (2021). Live-cell imaging of circadian clock protein dynamics in CRISPR-generated knock-in cells. Nat Commun *12*, 3796. https://doi.org/10.1038/s41467-021-24086-9.
41. Smyllie, N.J., Bagnall, J., Koch, A.A., Niranjan, D., Polidarova, L., Chesham, J.E., Chin, J.W., Partch, C.L., Loudon, A.S.I., and Hastings, M.H. (2022). Cryptochrome proteins regulate the circadian intracellular behavior and localization of PER2 in mouse suprachiasmatic nucleus neurons. Proc Natl Acad Sci U S A *119*. https://doi.org/10.1073/pnas.2113845119.
42. Novak, B., and Tyson, J.J. (2008). Design principles of biochemical oscillators. Nat Rev Mol Cell Biol *9*, 981-991. https://doi.org/10.1038/nrm2530.
43. Ferrell, James E., Jr., Tsai, Tony Y.-C., and Yang, Q. (2011). Modeling the Cell Cycle: Why Do Certain Circuits Oscillate? Cell *144*, 874-885. 10.1016/j.cell.2011.03.006.
44. Ferrell, J.E., Jr., and Ha, S.H. (2014). Ultrasensitivity part II: multisite phosphorylation, stoichiometric inhibitors, and positive feedback. Trends Biochem Sci *39*, 556-569. https://doi.org/10.1016/j.tibs.2014.09.003.
45. Lee, H., Chen, R., Lee, Y., Yoo, S., and Lee, C. (2009). Essential roles of CKIdelta and CKIepsilon in the mammalian circadian clock. Proc Natl Acad Sci U S A *106*, 21359-21364. https://doi.org/10.1073/pnas.0906651106.
46. Narasimamurthy, R., and Virshup, D.M. (2021). The phosphorylation switch that regulates ticking of the circadian clock. Molecular Cell *81*, 1133-1146. https://doi.org/10.1016/j.molcel.2021.01.006.
47. De Boeck, J., Rombouts, J., and Gelens, L. (2021). A modular approach for modeling the cell cycle based on functional response curves. PLoS Comput Biol *17*, e1009008. https://doi.org/10.1371/journal.pcbi.1009008.

48. Barrio, M., Leier, A., and Marquez-Lago, T.T. (2013). Reduction of chemical reaction networks through delay distributions. J Chem Phys *138*, 104114. https://doi.org/10.1063/1.4793982.
49. Park, S.J., Song, S., Yang, G.S., Kim, P.M., Yoon, S., Kim, J.H., and Sung, J. (2018). The Chemical Fluctuation Theorem governing gene expression. Nat Commun *9*, 297. https://doi.org/10.1038/s41467-017-02737-0.
50. Choi, B., Cheng, Y.Y., Cinar, S., Ott, W., Bennett, M.R., Josic, K., and Kim, J.K. (2020). Bayesian inference of distributed time delay in transcriptional and translational regulation. Bioinformatics *36*, 586-593. https://doi.org/10.1093/bioinformatics/btz574.
51. Kim, D.W., Hong, H., and Kim, J.K. (2022). Systematic inference identifies a major source of heterogeneity in cell signaling dynamics: The rate-limiting step number. Sci Adv *8*. https://doi.org/10.1126/sciadv.abl4598.
52. Tyson, J.J., and Novak, B. (2020). A Dynamical Paradigm for Molecular Cell Biology. Trends Cell Biol *30*, 504-515. https://doi.org/10.1016/j.tcb.2020.04.002.
53. Cai, X. (2007). Exact stochastic simulation of coupled chemical reactions with delays. J Chem Phys *126*, 124108. https://doi.org/10.1063/1.2710253.
54. Josic, K., Lopez, J.M., Ott, W., Shiau, L., and Bennett, M.R. (2011). Stochastic delay accelerates signaling in gene networks. PLoS Comput Biol *7*, e1002264. https://doi.org/10.1371/journal.pcbi.1002264.
55. Cao, Y., Wang, H., Ouyang, Q., and Tu, Y. (2015). The free energy cost of accurate biochemical oscillations. Nat Phys *11*, 772-778. https://doi.org/10.1038/nphys3412.
56. Qiao, L., Zhang, Z.-B., Zhao, W., Wei, P., and Zhang, L. (2021). Network design principle for robust oscillatory behaviors with respect to biological noise. bioRxiv, 2021.2012.2022.473835. https://doi.org/10.1101/2021.12.22.473835.
57. Li, Y., Shan, Y., Desai, R.V., Cox, K.H., Weinberger, L.S., and Takahashi, J.S. (2020). Noise-driven cellular heterogeneity in circadian periodicity. Proc Natl Acad Sci U S A *117*, 10350-10356. https://doi.org/10.1073/pnas.1922388117.
58. Abe, Y.O., Yoshitane, H., Kim, D.W., Kawakami, S., Koebis, M., Nakao, K., Aiba, A., Kim, J.K., and Fukada, Y. (2022). Rhythmic transcription of Bmal1 stabilizes the circadian timekeeping system in mammals. Nat Commun *13*, 4652. https://doi.org/10.1038/s41467-022-32326-9.
59. Gelens, L., Qian, J., Bollen, M., and Saurin, A.T. (2018). The Importance of Kinase-Phosphatase Integration: Lessons from Mitosis. Trends Cell Biol *28*, 6-21. 10.1016/j.tcb.2017.09.005.
60. Jin, M., Tavella, F., Wang, S., and Yang, Q. (2022). In vitro cell cycle oscillations exhibit a robust and hysteretic response to changes in cytoplasmic density. Proc Natl Acad Sci U S A *119*. 10.1073/pnas.2109547119.
61. Nomura, M., and Okada-Hatakeyama, M. (2013). Phase responses of oscillating components in a signaling pathway. Front Physiol *4*, 68. 10.3389/fphys.2013.00068.
62. Peercy, B.E., and Sherman, A.S. (2010). How Pancreatic β-Cells Discriminate Long and Short Timescale cAMP Signals. Biophysical Journal *99*, 398-406. https://doi.org/10.1016/j.bpj.2010.04.043.
63. Stevanovic, K., Yunus, A., Joly-Amado, A., Gordon, M., Morgan, D., Gulick, D., and Gamsby, J. (2017). Disruption of normal circadian clock function in a mouse model of tauopathy. Exp Neurol *294*, 58-67. https://doi.org/10.1016/j.expneurol.2017.04.015.
64. Mondragon-Rodriguez, S., Perry, G., Luna-Munoz, J., Acevedo-Aquino, M.C., and Williams, S. (2014). Phosphorylation of tau protein at sites Ser(396-404) is one of the earliest events in Alzheimer's disease and Down syndrome. Neuropathol Appl Neurobiol *40*, 121-135. https://doi.org/10.1111/nan.12084.
65. Hatfield, C.F., Herbert, J., van Someren, E.J., Hodges, J.R., and Hastings, M.H. (2004). Disrupted daily activity/rest cycles in relation to daily cortisol rhythms of home-dwelling

patients with early Alzheimer's dementia. Brain *127*, 1061-1074. https://doi.org/10.1093/brain/awh129.

66. Musiek, E.S. (2017). Circadian Rhythms in AD pathogenesis: A Critical Appraisal. Curr Sleep Med Rep *3*, 85-92. https://doi.org/10.1007/s40675-017-0072-5.
67. Kim, J.K., Josić, K., and Bennett, M.R. (2015). The relationship between stochastic and deterministic quasi-steady state approximations. BMC Systems Biology *9*, 87. https://doi.org/10.1186/s12918-015-0218-3.
68. Song, Y.M., Hong, H., and Kim, J.K. (2021). Universally valid reduction of multiscale stochastic biochemical systems using simple non-elementary propensities. PLoS Comput Biol *17*, e1008952. https://doi.org/10.1371/journal.pcbi.1008952.
69. Kim, J.K., and Tyson, J.J. (2020). Misuse of the Michaelis-Menten rate law for protein interaction networks and its remedy. PLoS Comput Biol *16*, e1008258. https://doi.org/10.1371/journal.pcbi.1008258.
70. Thomas, P., Straube, A.V., and Grima, R. (2012). The slow-scale linear noise approximation: an accurate, reduced stochastic description of biochemical networks under timescale separation conditions. BMC Syst Biol *6*, 39. https://doi.org/10.1186/1752-0509-6-39.
71. Kim, J.K., Josić, K., and Bennett, M.R. (2014). The Validity of Quasi-Steady-State Approximations in Discrete Stochastic Simulations. Biophysical Journal *107*, 783-793. https://doi.org/10.1016/j.bpj.2014.06.012.
72. Kim, J.K., and Sontag, E.D. (2017). Reduction of multiscale stochastic biochemical reaction networks using exact moment derivation. PLoS Comput Biol *13*, e1005571. https://doi.org/10.1371/journal.pcbi.1005571.
73. Gonze, D. (2013). Modeling the effect of cell division on genetic oscillators. Journal of Theoretical Biology *325*, 22-33. https://doi.org/10.1016/j.jtbi.2013.02.001.
74. Veliz-Cuba, A., Hirning, A.J., Atanas, A.A., Hussain, F., Vancia, F., Josić, K., and Bennett, M.R. (2015). Sources of Variability in a Synthetic Gene Oscillator. PLOS Computational Biology *11*, e1004674. https://doi.org/10.1371/journal.pcbi.1004674.
75. Paijmans, J., Lubensky, D.K., and Rein Ten Wolde, P. (2017). Robustness of synthetic oscillators in growing and dividing cells. Phys Rev E *95*, 052403. https://doi.org/10.1103/PhysRevE.95.052403.